J. Fluid Mech. (1993), vol. 254, pp. 267–281

Direct numerical calculation of acoustics: solution evaluation through energy analysis

By KENNETH S. BRENTNER
MS 461, NASA Langley Research Center, Hampton, VA 23681, USA

(Received 24 August 1992 and in revised form 5 March 1993)

The propagation of acoustic energy from a sound source to the far field is a fundamental problem of acoustics. In this paper the use of computational fluid dynamics (CFD) to directly calculate the acoustic field is investigated. The two-dimensional, compressible, inviscid flow about an accelerating circular cylinder is used as a model problem. The time evolution of the energy transfer from the cylinder surface to the fluid, as the cylinder is moved from rest to some non-negligible velocity, is shown. Energy is the quantity of interest in the calculations since various components of energy have physical meaning. By examining the temporal and spatial characteristics of the numerical solution, a distinction can be made between the propagating acoustic energy, the convecting energy associated with the entropy change in the fluid, and the energy following the body. In the calculations, entropy generation is due to a combination of physical mechanisms and numerical error. In the case of propagating acoustic waves, entropy generation seems to be a measure of numerical damping associated with the discrete flow solver.

1. Introduction

The process of rapidly accelerating a body can be a potent noise source. It is natural then to consider the transient behaviour of the compressible flow field in this situation. Several model problems have been studied analytically for various limiting conditions. Ffowcs Williams & Lovely (1977) considered the case of a sphere that is suddenly brought into a low Mach number translation in an inviscid, compressible fluid. G. I. Taylor (1942) also considered a sphere which, after an impulsive start, decelerated due to the drag induced by the transient pressure field. When the sphere is impulsively started to low Mach number, both of these studies found an equipartitioning of the energy between the kinetic energy following the body and the radiated acoustic energy. Longhorn (1952) found that the work required to start a sphere impulsively was twice the amount needed if the sphere was started slowly. The additional work required to rapidly accelerate the sphere supplies the energy which radiates as sound for this low Mach number problem.

Although low Mach number problems have been treated, transonic flows are difficult to handle analytically with any generality. In this paper, the Euler equations, together with the continuity and energy equations, are solved numerically for the two dimensional model problem of a circular cylinder accelerating from rest. The Euler equations were chosen so that the artificially viscous nature of the discrete numerical algorithm may be considered independently from real viscous effects. The Euler equations are also useful because they allow strong shock waves and the transport of vorticity.

2. The accelerating cylinder

Inspired by the accelerating sphere problem, an investigation of the transient flow field around a circular cylinder which has impulsively started is now given. Leftward translation at Mach 0.4, approximately the critical Mach number for the cylinder, was chosen so that the flow around the cylinder would be transonic without having shock waves in the ultimate steady flow.

2.1. *Numerical method*

The Euler equations were chosen as the appropriate set of governing equations since they can describe the physical characteristics of both sound and shock waves. The inherent numerical viscosity of the discrete solution is suspected of adversely affecting the calculated acoustic field. Any viscous phenomenon observed in the present Euler calculations must be related to the numerical solution procedure.

The Euler code developed for this work uses a moving computational grid, hence in the computations the body is moving through a stationary fluid. The dependent variables are specified in a reference frame fixed to the undisturbed medium. The vectorial form of the Euler equations, together with continuity and energy, may be written in conservation form as

$$\frac{\partial \boldsymbol{U}}{\partial t} + \mathrm{V}_{\boldsymbol{X}} \cdot \vec{\boldsymbol{F}} = 0, \tag{2.1}$$

where

$$\boldsymbol{U} = \begin{Bmatrix} \rho \\ \rho u \\ \rho v \\ \rho E \end{Bmatrix} \quad \text{and} \quad \vec{\boldsymbol{F}} = \boldsymbol{U}(\vec{q} - \vec{v}) + p \begin{Bmatrix} 0 \\ \hat{i} \\ \hat{j} \\ \vec{q} \end{Bmatrix}$$

for a reference frame moving with velocity $\vec{v}$. Here $\boldsymbol{U}$ is the vector of dependent variables – density, momentum, and total energy; $\vec{q}$ is the fluid velocity (u, v); $\vec{v}$ is the velocity of the body and grid; and $\hat{i}, \hat{j}$ are the unit vectors in the usual coordinate directions. In (2.1), the subscript $\boldsymbol{X}$ indicates that the spatial independent variables are in the moving frame. The $\boldsymbol{U}\vec{v}$ term in the flux matrix $\vec{\boldsymbol{F}}$ arises from the time derivative of the moving coordinates. Since these additional terms will always be apparent in the flux matrix when the reference frame is moving, the subscript $\boldsymbol{X}$ will not be included in subsequent equations. A moving grid was chosen to simplify the treatment for an accelerating body.

A finite-volume method with multistage time stepping of the Jameson type was used to solve the two-dimensional Euler equations (see Jameson, Schmidt & Turkel 1981; Schmidt & Jameson 1982; Jameson & Schmidt 1985). The present implementation is a cell centred scheme, taken directly from Schmitz & Jameson (1982), which is second-order-accurate in space and time. To maintain time accuracy, none of the usual steady-state convergence acceleration techniques were used. The semi-discrete form of (2.1) can be written

$$\frac{\mathrm{d}}{\mathrm{d}t}\left(\boldsymbol{U}_{ij} \Delta V_{ij}\right) + \boldsymbol{Q}_{ij} - \boldsymbol{D}_{ij} = 0, \tag{2.2}$$

where $\boldsymbol{Q}_{ij}$ is the convective flux balance vector for the ijth grid cell and $\boldsymbol{D}_{ij}$ is the added dissipative term for the same cell. The dissipation used in this work was Jameson's adaptive combination of second and fourth differences (Schmidt & Jameson 1982, equation 12–17; Jameson & Schmidt 1985, equation 4.6a). The fourth differences provides a low level of third-order background dissipation while the second

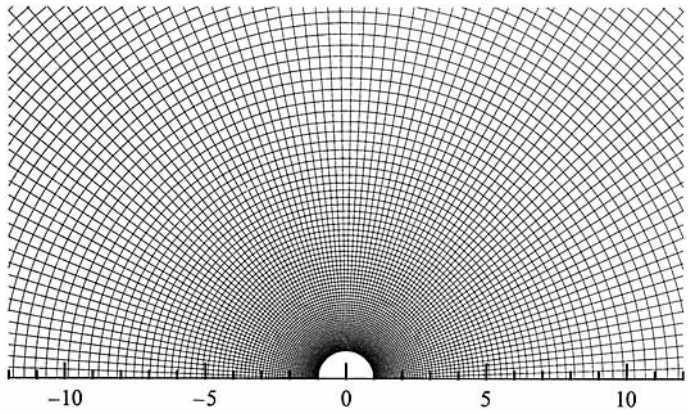

FIGURE 1. The inner part of the computational grid used for the numerical calculations.

differences make the scheme behave like a first-order method near shocks. A five-stage, Runge–Kutta-like, time-stepping scheme is used for the explicit time integration. The dissipative terms were evaluated only in the first two stages to reduce the number of computations. Non-reflecting boundary conditions, based on the extrapolation of the linearized characteristic variables, are used at the outer computational boundaries (Schmidt & Jameson1982). The surface boundary conditions consist of a statement of no flow through the body surface together with a linear extrapolation of the pressure onto the surface. Symmetry is assumed between the upper and lower half-planes, therefore computations are carried out only in the upper half-plane and symmetry boundary conditions are applied on the x-axis.

The computational grid used for these calculations is a polar grid which models half of the flow field and moves with the cylinder. The azimuthal direction is divided into 95 cells ($\Delta\theta = 0.0331$ radians). The radial dimension of the grid cells increases linearly up to ten cylinder radii from the centre of the cylinder, after which the radial increment remains constant out to forty cylinder radii (the outer boundary of the grid). Figure 1 shows the inner part of the computational domain. Notice the grid has very fine resolution, especially near the cylinder surface. More details of the Euler code used for these calculations is given by Brentner (1990).

2.2. *Description of the starting process*

As the cylinder impulsively starts moving leftward, an expansion wave propagates to the right, behind the cylinder, while a compression wave moves to the left, ahead of the cylinder. This is shown in the time sequence of density perturbation contours plotted in figure 2. The density perturbation, ρ', is scaled by $r_o^{\frac{1}{2}}$ to account for the effect of cylindrical spreading. Here r_o is the distance from the point in the field to the position where the cylinder centre was located a time $t = 0$. Notice that the expansion moves away from the cylinder more quickly than the compression. This is due to the relative motion of the cylinder. The steady flow field near the cylinder surface is established by the non-dimensional time $t = 20$. Note that in all the contour plots, the range of contours is limited: therefore the extreme values in the contour plot may be greater than the maximum or less than the minimum shown in the legend.

Immediately after the impulsive start, the pressure on the surface corresponds to $p = p_o + \rho_o c_o v_n$, which is expected for an impulsive motion. (Here the subscript o refers to the undisturbed fluid state and v_n is the normal component of the local

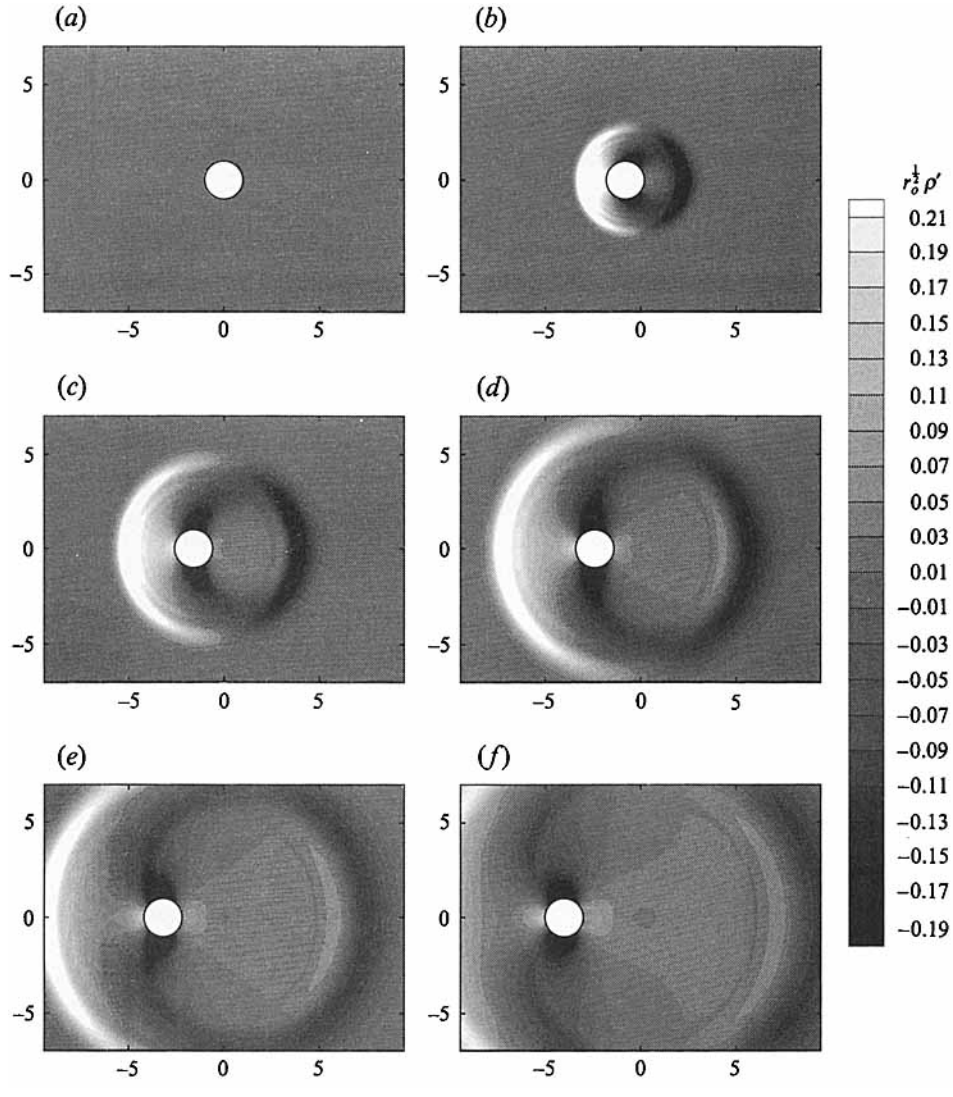

FIGURE 2. Density perturbation ρ' contours for a cylinder impulsively started to Mach 0.4. The density perturbation has been scaled by $r_o^{\frac{1}{2}}$ to account for cylindrical spreading. (*a*) $t = 0.11$; (*b*) $t = 2.0$; (*c*) $t = 4.0$; (*d*) $t = 6.0$; (*e*) $t = 8.0$; (*f*) $t = 10.0$.

surface velocity.) Subsequently a shock forms on the downstream side of the cylinder, strengthens, and moves forward. As the shock reaches the top of the cylinder, it begins to weaken as it continues to move forward until it finally leaves the cylinder surface. Shortly after the shock leaves the cylinder region, the flow field around the cylinder approaches that expected for a steady potential flow. The non-circulatory steady-state solution for a potential flow is unique. Hence it does not depend upon the time history, but the transient flow field and the work required to maintain the cylinder velocity during the transient phase vary greatly with the manner in which the steady-state flow is achieved. This will be discussed in more detail later.

2.3. *Energy partition*

With a qualitative understanding of the physics, it is useful to discuss the problem more quantitatively. Longhorn (1952) has done this using the total work required to accelerate a sphere to low Mach number translation as a quantitative measure. The work required to accelerate the cylinder gives a measure of energy input into the system. Once in the fluid, the energy can be separated into its various components. Energy flux out of a control volume enclosing the cylinder can be used to determine the propagation and convection of energy to the far field. The form in which energy leaves the control volume can be determined by the time required to exit the volume, since the acoustic propagation and fluid convection speeds are disparate.

Myers (1991) has recently developed an exact energy corollary which is well suited for consideration of energy transport in flow fields which may include shock waves and vorticity. Myers' result is a generalization of the concept of acoustic energy, which he recognized from a perturbation expansion of the general energy equation of fluid mechanics. Since this corollary is exact, it is uniquely appropriate for the nonlinear problems under current consideration. For the case of perturbation about an undisturbed inviscid fluid, Myers' corollary can be written as

$$\frac{\partial \varepsilon}{\partial t} + \nabla \cdot \vec{\mathscr{F}} = 0, \tag{2.3}$$

where

$$\varepsilon = \rho\left(\Delta h + \frac{u^2}{2} - T_o \Delta s\right) - \Delta p \tag{2.4}$$

and

$$\vec{\mathscr{F}} = \rho\left(\Delta h + \frac{u^2}{2} - T_o \Delta s\right)\vec{q}. \tag{2.5}$$

In these equations, h is the specific enthalpy, $e + p/\rho$, and s is the specific entropy. The subscript o refers to the value of the quantity in the undisturbed medium and $\Delta(\,) = (\,) - (\,)_o$. This is a substantially simplified version of Myers' result since the effect of mean flow, viscosity, and heat conduction have been neglected.

The energy density given in (2.4) contains three components,

$$\varepsilon_k = \frac{\rho u^2}{2}, \tag{2.6}$$

$$\varepsilon_p = \rho(\Delta h - T_o \Delta s) - \Delta p, \tag{2.7}$$

$$\varepsilon_s = \rho T_o \Delta s, \tag{2.8}$$

which are the kinetic, potential, and entropy energy densities, respectively. The kinetic energy has its normal physical meaning and is the only component of energy in the inviscid, incompressible limit. The potential energy is related to the compression of the fluid, and the entropy energy is energy corresponding to the increase of entropy in the fluid. Notice that each of these energy density terms are defined such that their value is zero in the undisturbed fluid and the sum $\varepsilon_k + \varepsilon_p$ is ε in (2.4). A statement of energy conservation, written in terms of these components in a reference frame moving with velocity $\vec{v}$, is

$$\frac{\partial}{\partial t}[\varepsilon_k + \varepsilon_p + \varepsilon_s] + \nabla \cdot \left[(\varepsilon_k + \varepsilon_p + \varepsilon_s - p_o)(\vec{q} - \vec{v}) + p\vec{q}\right] = 0. \tag{2.9}$$

Upon integration over a control volume and using the divergence theorem, the global

conservation of energy statement can be written in component form as

$$\frac{\partial}{\partial t}(E_k + E_p + E_s) + \dot{F}_a + \dot{F}_s = \dot{W} \tag{2.10}$$

by defining

$$E_k = \int_V \varepsilon_k \, \mathrm{d}V, \tag{2.11}$$

$$E_p = \int_V \varepsilon_p \, \mathrm{d}V, \tag{2.12}$$

$$E_s = \int_V \varepsilon_s \, \mathrm{d}V, \tag{2.13}$$

$$F_a = \int_{t_o}^{t} \int_{g=0} \left[(\varepsilon_k + \varepsilon_p - p_o)(q_n - v_n) + pq_n\right] \mathrm{d}S\mathrm{d}\tau, \tag{2.14}$$

$$F_s = \int_{t_o}^{t} \int_{g=0} \varepsilon_s(q_n - v_n) \, \mathrm{d}S\mathrm{d}\tau, \tag{2.15}$$

$$W = \int_{t_o}^{t} \int_{f=0} pv_n \, \mathrm{d}S\mathrm{d}\tau. \tag{2.16}$$

Here E_k, E_p, and E_s refer to the total amount of kinetic, potential, and entropy energy in the volume at a particular time. F_a and F_s are the time-integrated flux of acoustic and entropy energy out of the volume (i.e. through the outer boundary of the volume) since time $t = -\infty$, and W is the total work done by the body on the fluid since $t = -\infty$. The dot over F_a, F_s and W in (2.10) represents time differentiation and is used only on boundary integrals. These global measures of energy are also useful for quantitatively examining the transfer of energy from the cylinder surface to the fluid and ultimately the far field. A more precise definition of these quantities is given by Brentner (1990).

2.4. *Energy distribution*

The components of energy discussed in the previous section are now used to develop an understanding of the energy transport from the cylinder surface to the near and far fields after a Mach 0.4 impulsive start. In figures 3, 4, and 5, the kinetic, potential, and entropy energy density contours are plotted in a time sequence. Note that the energy density is scaled by r_o to account for cylindrical spreading of the energy as it propagates away from the cylinder surface. Figure 3 shows that the kinetic energy is concentrated both near the cylinder surface and in the acoustic wavefronts. The kinetic energy following the cylinder, which is part of the local aerodynamic field, distributes itself more or less uniformly around the cylinder. The kinetic energy component of the acoustic energy radiates mainly to the left and right of the cylinder, with the highest intensity forward of the cylinder in the direction of the motion. The shock can be seen in the local kinetic energy distribution as a discontinuity in the contours near the cylinder, from $t = 4.0$ to $t = 8.0$, in figure 3($c - e$).

As in the case of the kinetic energy, the potential energy is found primarily in

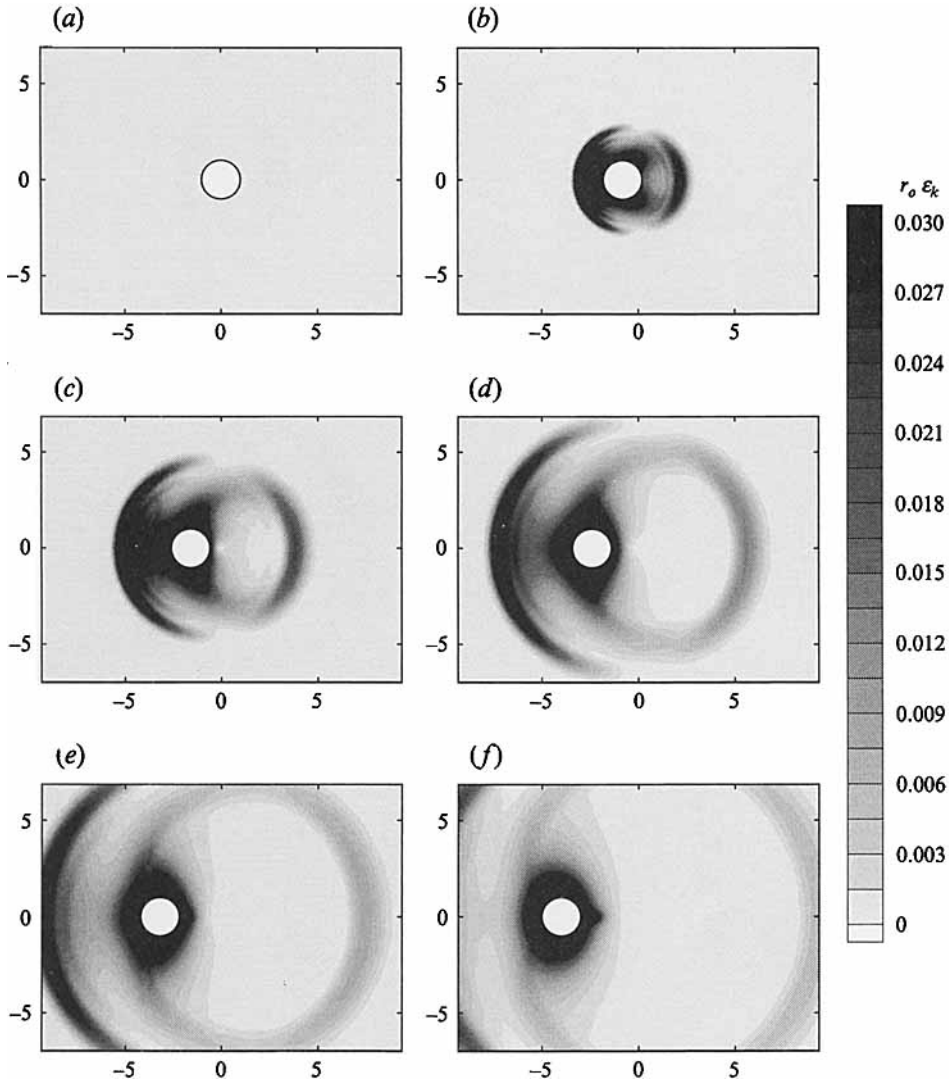

FIGURE 3. Kinetic energy field ε_k for a cylinder impulsively started to Mach 0.4 translation. Energy has been scaled by r_o to account for cylindrical spreading. (*a*) $t = 0.11$; (*b*) $t = 2.0$; (*c*) $t = 4.0$; (*d*) $t = 6.0$; (*e*) $t = 8.0$; (*f*) $t = 10.0$.

the wave fronts and near the cylinder, but unlike kinetic energy, the potential energy following the cylinder is found predominantly in the region of maximum fluid velocity. The shock is much more apparent in the potential energy density contour sequence shown in figure 4. This is to be expected since the potential energy in the fluid identifies the presence of compressibility. For a low Mach number flow, the potential energy contribution to the local field following the body, i.e. the aerodynamic field, would be negligible compared with the kinetic energy. Hence the potential energy would be primarily of interest in the acoustic waves. A comparison of figures 3 and 4 reveals that the energy in the acoustic waves, both the compression and expansion, is nearly equally divided between kinetic and potential energy components.

The contours of entropy energy density, shown in figure 5, reveal an unexpected

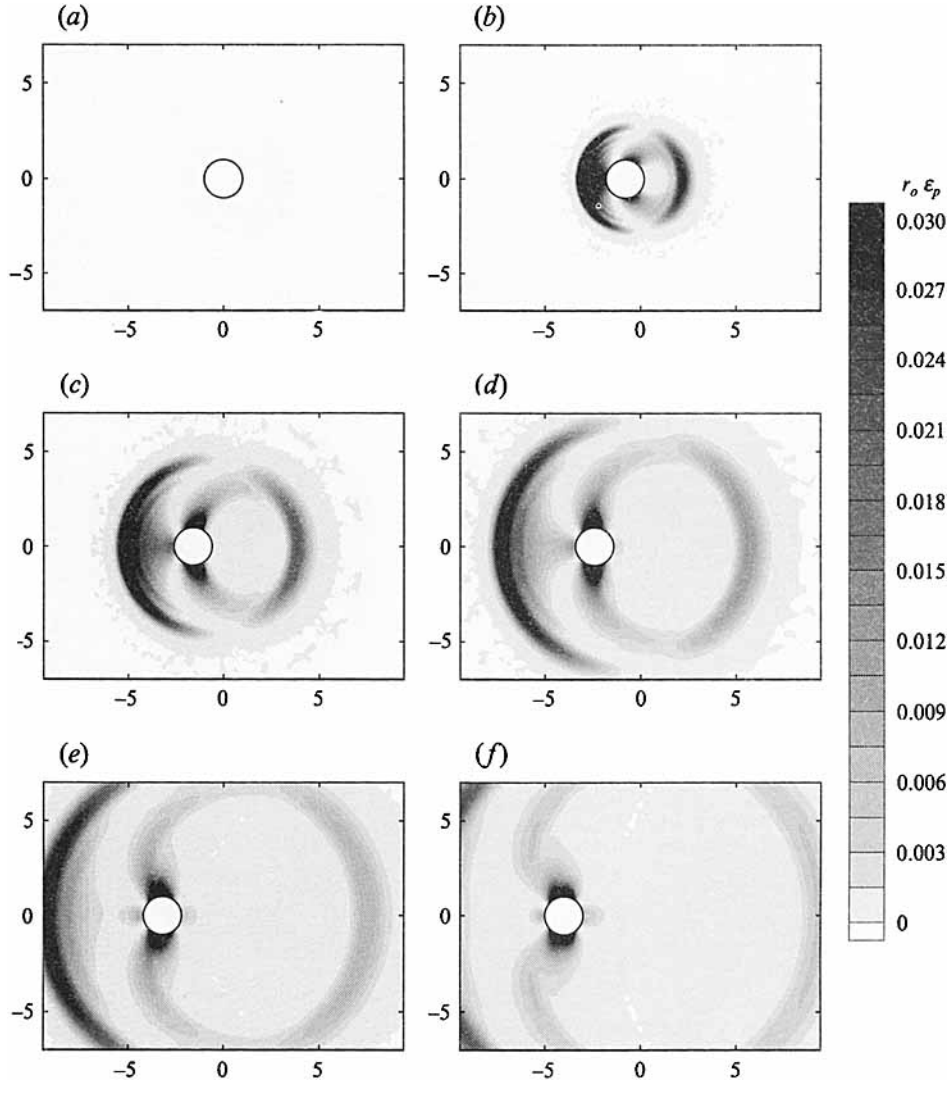

FIGURE 4. Potential energy field ε_p for a cylinder impulsively started to Mach 0.4 translation. Energy has been scaled by r_o to account for cylindrical spreading. (*a*) $t = 0.11$; (*b*) $t = 2.0$; (*c*) $t = 4.0$; (*d*) $t = 6.0$; (*e*) $t = 8.0$; (*f*) $t = 10.0$.

relationship between the acoustic waves and entropy in the numerical solution. This is unexpected since sound propagation is an essentially inviscid, *isentropic* process. Upon closer examination of figure 5, it is evident that the area of the highest level of entropy energy remains near the surface of the cylinder for the short time sequence shown in the figure. This concentrated region of entropy highlights a vortex generated by the strong transient shock which exists shortly after the start of motion. Even so, the most striking feature is the undeniable entropy generation by the propagating acoustic waves – a phenomenon which must have numerical rather than physical origins. This result suggests that the numerically induced errors or damping are identified by the entropy energy term. The significance of this finding is that entropy energy gives a quantitative local measure of the numerical error which can be used

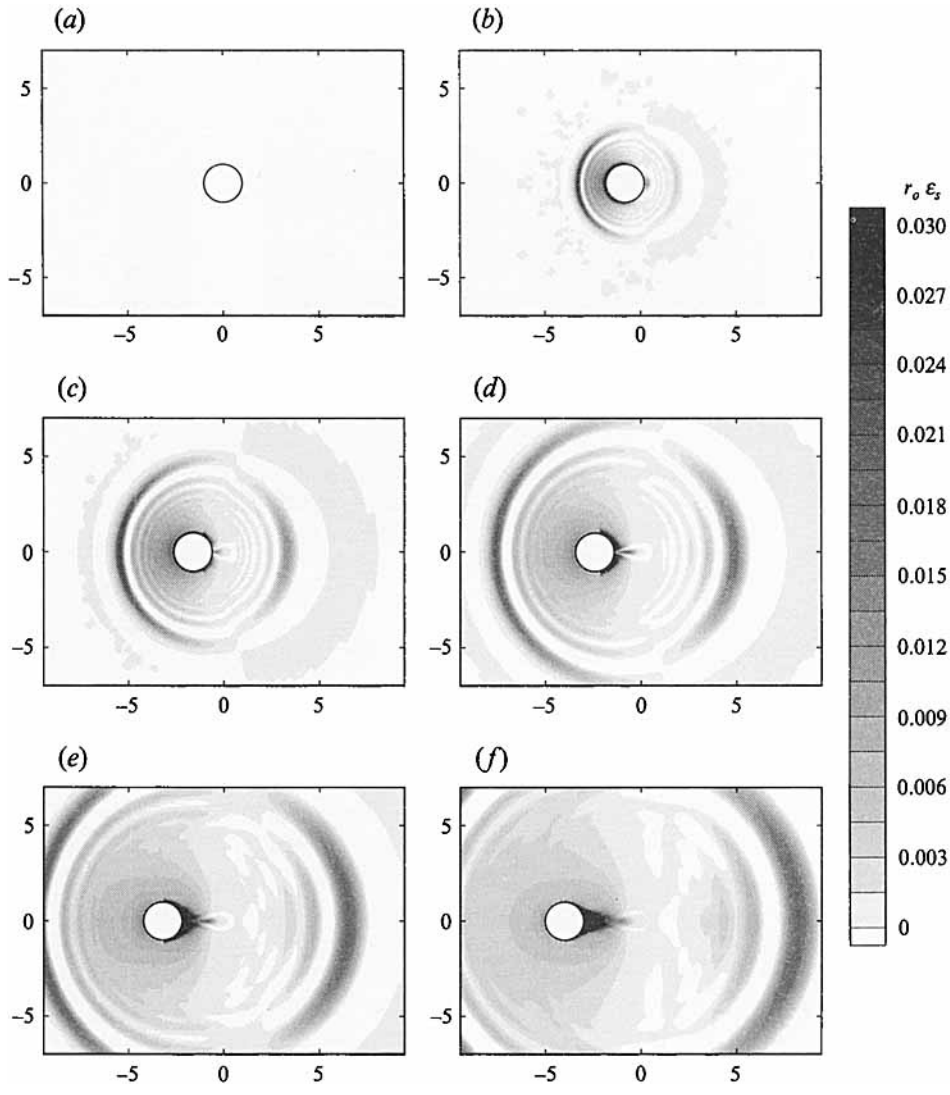

FIGURE 5. Entropy energy field ε_s for a cylinder impulsively started to Mach 0.4 translation. Energy has been scaled by r_o to account for cylindrical spreading. (*a*) $t = 0.11$; (*b*) $t = 2.0$; (*c*) $t = 4.0$; (*d*) $t = 6.0$; (*e*) $t = 8.0$; (*f*) $t = 10.0$.

to judge the acceptability of the acoustic solution. This idea is central to this paper and shall be considered in more detail in what follows.

2.5. *Global energy balance*

With a better understanding of how the components of energy are spatially and temporarily distributed, it is useful to consider the global energy balance as a function of time for a control volume surrounding the cylinder. In the following calculations, a circular control surface, with a radius of ten cylinder radii and concentric with the cylinder at each time, defines a volume around the cylinder. The total kinetic, potential, and entropy energy in the volume along with the acoustic and entropy energy flux out of the volume, indicated in (2.10), are computed as a function of time for various starting scenarios.

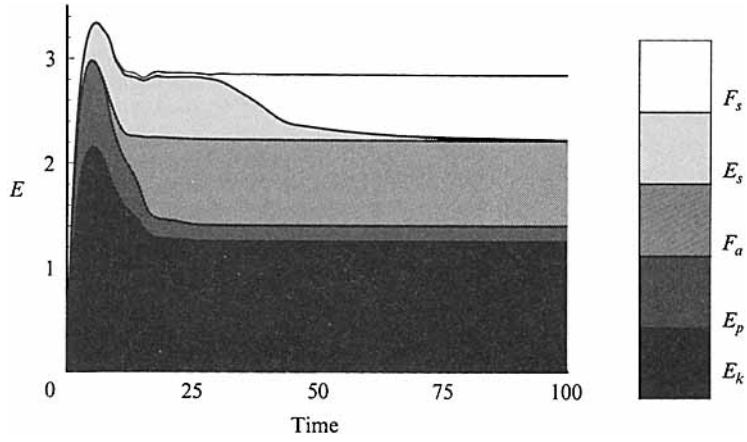

FIGURE 6. Global energy balance time history for a cylinder impulsively started to $M = 0.4$. The control volume radius is $R = 10$. The total kinetic energy E_k, potential energy E_p, acoustic energy flux F_a, entropy energy E_s, and entropy energy flux F_s are non-dimensionalized by the total incompressible kinetic energy, $\rho\pi R^2 v^2/2$.

In figures 6 and 7, the energy components are added such that the envelope of the curves represents the total work input into the fluid by the cylinder. Each of the components is non-dimensionalized by the total kinetic energy of the incompressible case, $\rho\pi a^2 v^2/2$. When the total work is calculated independently, using the computed pressure on the cylinder surface, it is nearly indistinguishable from the envelope of the energy components. Notice that kinetic energy, potential energy and acoustic energy flux are the first three components in figures 6 and 7. They are plotted in this order because acoustic energy is counted as kinetic and potential energy while inside the control volume and acoustic energy flux as it leaves the control volume. Likewise entropy energy and entropy energy flux are plotted together since they correspond to the same component of energy either inside or outside of the specified volume.

When the cylinder is impulsively started to Mach 0.4, most of the work goes initially into kinetic and potential energy modes and eventually a significant entropy energy component before $t = 6.4$ at which time acoustic energy begins to leave the control volume. This is shown in figure 6. By time $t = 36.0$, all of the acoustic energy has left and the entropy energy begins to leave. The entropy energy convects with the fluid velocity rather than the sound speed, thus accounting for the delay in leaving the control volume. Acoustic waves have completely left the control volume when the acoustic flux contribution reaches its final constant value. Notice in figure 6 that there is apparently no increase in the total system entropy after time $t = 15$, which corresponds to the time when nearly all the acoustic waves have left the control volume. This is another indication that acoustic energy is being dissipated in the discrete numerical calculation.

Figure 6 also shows that total energy input into the fluid after an impulsive start is equally divided between the kinetic and potential energy, which follow the body, and the acoustic and entropy energy, which are transported to the far field. This finding is consistent with the low Mach number theory for the sphere (Taylor 1942; Longhorn 1952; Ffowcs Williams & Lovely 1977) and is an extension of previous results since the numerical computations have no restriction to low Mach number. In fact the transient flow field is transonic, vorticity is generated, and there is significant

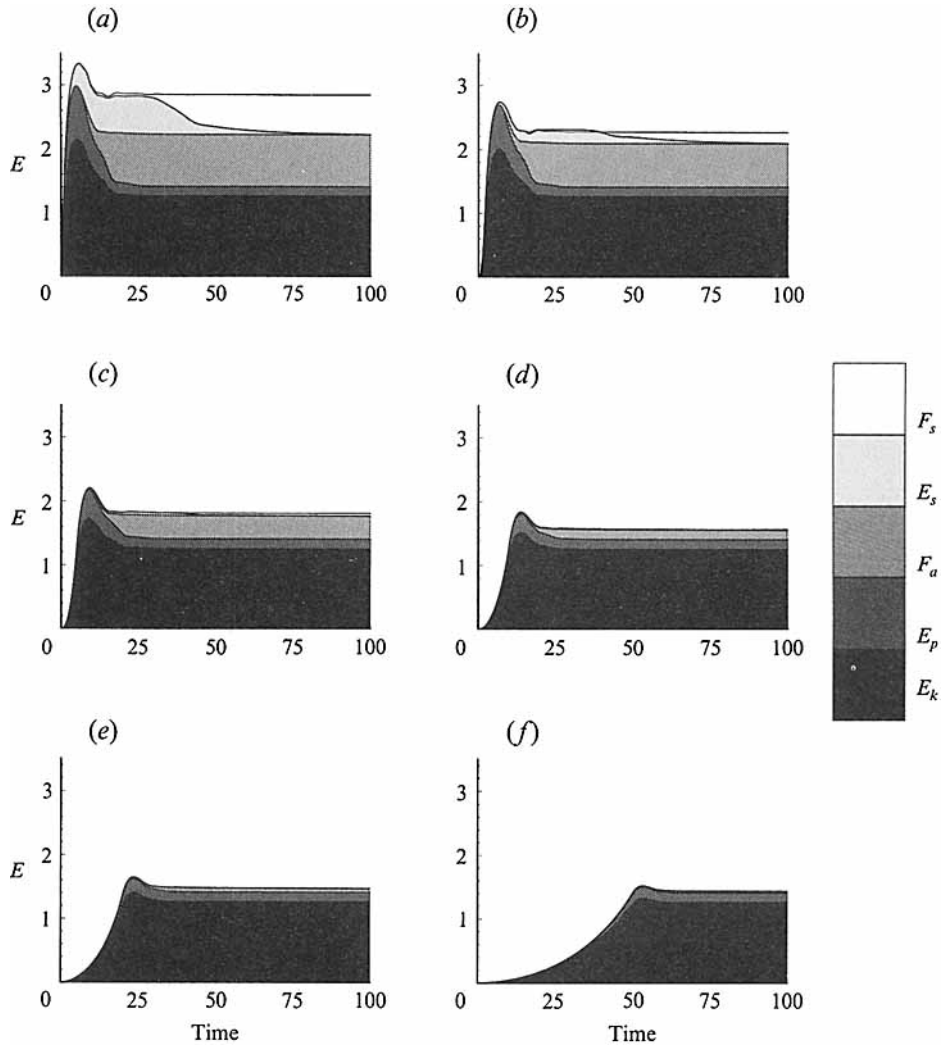

FIGURE 7. Global energy balance time history for a control volume with radius $R = 10$. The total kinetic energy E_k, potential energy E_p, acoustic energy flux F_a, entropy energy E_s, and entropy energy flux F_s are non-dimensionalized by the total incompressible kinetic energy, $\rho\pi R^2 v^2/2$, where v is the steady-state velocity Mach 0.4. (*a*) impulsive start; (*b*) acceleration = 1/5; (*c*) acceleration = 2/25; (*d*) acceleration = 1/25; (*e*) acceleration = 2/125; (*f*) acceleration = 1/125.

potential energy even in the ultimate steady aerodynamic field. Based on figure 6, the equipartition of energy is no longer simply a balance between the kinetic energy in the local field and the acoustic energy propagating to the far field as in the low Mach number case. After the impulsive start, half of the input energy remains near the cylinder and the other half goes to the far field. The local energy field is comprised of both kinetic and potential energy while both acoustic propagation and entropy convection account for the energy transport to the far field in the more general case of compressible flow.

Figure 7 ($b - f$) shows the energy transfer for a cylinder accelerated at various non-impulsive, constant non-dimensional acceleration rates. An examination of

figure 7($a - f$) reveals that the total work input at steady-state (the sum of all the energy components at large time) declines significantly with reduced acceleration even though the steady-state flow field is the Mach 0.4 potential flow solution for each case. As the rate of acceleration is decreased, the production of entropy and acoustic energies declines until for the case of very low acceleration in figure 7(f), the energy input into the fluid nearly corresponds to the energy in the local field. Only a very small amount of acoustic energy is generated in the process. Also note in the figure that the entropy generated is greatly reduced when the acceleration rate is decreased.

3. Sources of entropy

One nagging question must still be addressed – How much of the entropy energy results from numerical error and how much is real? For the impulsively started cylinder, both physical and numerical entropy generation mechanisms must be present. The physical source of entropy in this inviscid calculation is the strong shock generated during the transient startup period. The exact mechanism responsible for the numerical dissipation of the acoustic waves is not fully understood. This is clearly a serious problem since the desired numerical calculation should mimic the isentropic nature of the physical situation. There is some hope that this will not be an insurmountable problem, however, since for lower acceleration rates there is very little energy in the entropy component even though there is still a significant acoustic energy component. (See figure 7c for example.) Hence even if acoustic energy is dissipated, it may be at negligible levels. In the remainder of this paper, an investigation will be made to determine the source of the non-physical origins of the entropy. Specifically, the effect of the explicitly added artificial viscosity and the role of grid resolution will be studied separately.

3.1. *Effect of artificial viscosity*

The artificial viscosity added for numerical stability seems to be an obvious generator of unwanted entropy. The form of the artificial dissipation used in the computations is that given by Schmidt & Jameson (1982) and Jameson & Schmidt (1985). It is composed of a combination of second and fourth differences, with the fourth differences providing background dissipation and the second differences adaptively turned on in regions of sufficiently high gradients. The purpose of the second differences in the dissipation is to eliminate oscillations around shock waves, but the present form of the scheme does not necessarily distinguish between shock waves and acoustic waves. To examine the amount of entropy generation by the artificial viscosity terms, the magnitude of the dissipation terms were increased independently. In figure 8(a), the effect of changing the damping coefficients on the entropy energy is shown. Even when the second-differences term is tripled or the fourth-differences term is increased by an order of magnitude, the effect on entropy generation is minimal.

3.2. *Effect of grid resolution*

The grid resolution is certainly related to the numerical dissipation observed in the calculations. In fact, the grid probably does not sufficiently resolve the high-frequency component of the acoustic waves generated during the impulsive start. The high level of entropy energy observed in the impulsive case may be an indication of this. To study this effect, three additional computational grids are considered. The grid used in the previous calculations and shown in figure 1 is designated here as Grid 1. Grid 2 has half the resolution of Grid 1 in both the r- and θ-directions while Grids 3 and 4

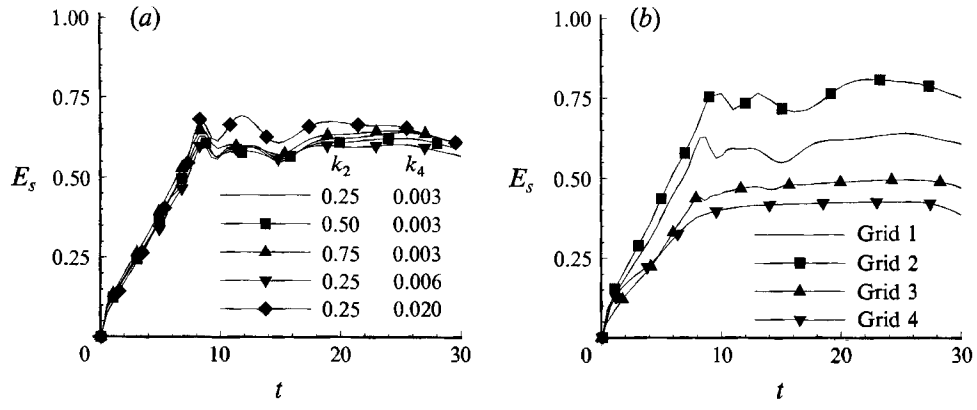

FIGURE 8. A comparison of the entropy energy E_s in the control volume for various levels of the artificial viscosity and different grids. The nominal values of the coefficients of the second and fourth differences in the viscosity are $k_2 = 0.25$ and $k_4 = 0.003$, respectively. Grid 1 is the nominal grid. (*a*) Effect of artificial viscosity; (*b*) effect of grid resolution.

both have significantly finer resolution in the r-direction. The constant radial spacing of Grid 4 starts at a much smaller r than the other grids, giving it the finest radial resolution. Grid 3 has twice the azimuthal resolution of Grid 1 and Grid 4. The ratio between the temporal and spatial discretization sizes (CFL number) was held constant for all grids by changing the time step to account for changes in the grid size.

The grid resolution seems directly related to the entropy level, as shown in figure 8(*b*). The coarser grid has a high level of entropy corresponding to a loss in acoustic energy while the entropy of the finer grids is significantly reduced. Upon closer examination of the solution, the amount of entropy computed using the fine grids seems to be near that which was physically generated by the shock immediately after startup. Figure 9 compares the entropy energy distribution for the impulsively started cylinder at time $t = 8.0$. Notice that both Grids 3 and 4 have significantly less entropy energy associated with the acoustic waves than the original grid. These calculations agree with the prevailing view that very high accuracy is required for the prediction of acoustics. Thus grid resolution and the order of accuracy of the numerical algorithm are of primary importance in direct computation of acoustics with CFD methods.

Even though grid refinement improved the calculations, a polar grid is not be the best choice since the azimuthal arclength of the cells grows linearly with r. Other types of grids which maintain the grid cell size uniformly throughout the computational domain are more suitable for acoustics since they minimize the effects of grid stretching. Perhaps adaptive, unstructured grids can be used to actually increase the grid density only where waves exist in the field. Higher-order-accuracy algorithms are also needed to reduce the demand for extremely fine grids. Finally, the local energy field seems to be much less sensitive to the grid resolution than the field away from the body – an observation which explains why stretched grids do not seem to cause problems in aerodynamic calculations.

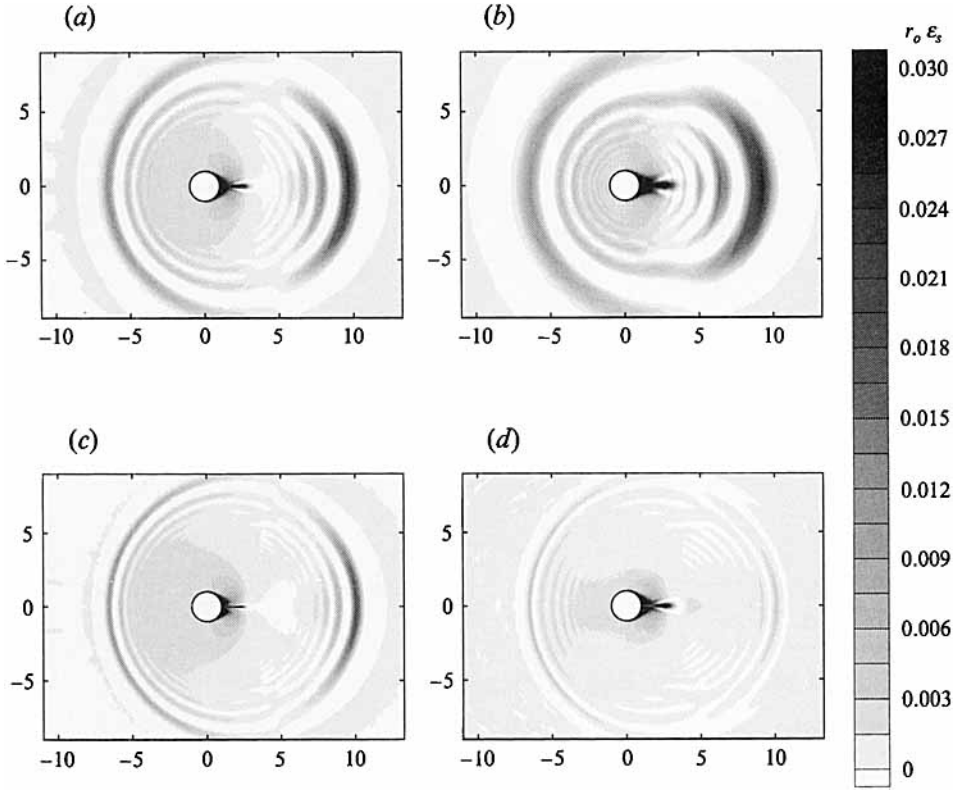

FIGURE 9. A comparison of the entropy energy ε_s distribution for various grids at $t = 8.0$. The cylinder was impulsively started in Mach 0.4 translational motion. (*a*) Grid 1; (*b*) grid 2; (*c*) grid 3; (*d*) grid 4.

4. Conclusions

The aim of this paper is twofold: (i) to understand the nonlinear, transient energy transfer from the surface of an accelerating cylinder to the far field; and (ii) to better understand the capabilities and limitations of present day CFD methodology as applied to acoustic problems. Both of these aims have been addressed through the numerical study of the circular cylinder model problem.

The transition from rest to a Mach 0.4 translation is somewhat more complicated than in the low Mach number problems studied previously. When the cylinder is accelerated rapidly, a shock forms in the compressible fluid, generating entropy and vorticity in the early stages of the motion. As the shock disappears, the vorticity convects away from the cylinder and the steady flow around the cylinder becomes essentially potential. It is somewhat surprising then that an equipartition of energy exists for this compressible problem in the same way as a low Mach number case. Nevertheless, the present calculations show that half of the energy input during an impulsive start follows the cylinder and the other half is transported to the far field.

Finally, the separation of energy into kinetic, potential, and entropy energy components is useful in understanding both the physics of the problem and the effect of the numerical damping. The entropy term is especially useful because it gives a quantitative measure for comparing the effect of algorithms and grids on the unsteady solution. This use of energy is apparently new. For the second-order-accurate,

finite-volume, Euler solutions computed for this paper, the discretization errors related to the grid resolution appear to be the primary source of numerically generated entropy. If the grid is too coarse, acoustic energy is transferred to entropy energy as it propagates. The role of the explicitly added artificial viscosity has a small effect on the time-dependent energy solution.

This research was carried out under the supervision of Professor J. E. Ffowcs Williams as part of the author's doctoral work.

REFERENCES

BRENTNER, K. S. 1990 The sound of moving bodies. Ph.D. dissertation, University of Cambridge.

FFOWCS WILLIAMS, J. E. & LOVELY, D. J. 1977 An approximate method for evaluating the sound of impulsively accelerated bodies. *J. Sound Vib.* **50**, 333-343.

JAMESON, A. & SCHMIDT, W. 1985 Some recent developments in numerical methods for transonic flows. *Comp. Meth. Appl. Mech. Engng* **51**, 467-493.

JAMESON, A., SCHMIDT, W. & TURKEL, E. 1981 Numerical solution of the euler equations by finite volume methods using Runge-Kutta time-stepping schemes. *AIAA Paper 81-1259.*

LONGHORN, A. L. 1952 The unsteady, subsonic motion of a sphere in a compressible inviscid fluid. *Q. J. Mech. Appl. Maths* **V**, 64-81.

MYERS, M. K. 1991 Transport of energy by disturbances in arbitrary steady flows. *J. Fluid Mech.* **226**, 383-400.

SCHMIDT, W. & JAMESON, A. 1982 Recent developments in finite-volume time-dependent techniques for two and three dimensional transonic flows. *Von Karman Lecture Series* 1982-04.

TAYLOR, G. I. 1942 The motion of a body in water when subjected to a sudden impulse. In *Scientific Papers of G. I. Taylor* (ed. G. K. Batchelor), vol. 3, pp. 306-308. Cambridge University Press.